ENERGETIKA. 2024
T. 70. Nr. 1. P. 29–40
ISSN 0235-7208 eISSN 1822-8836
DOI: https://doi.org/10.6001/energetika.2024.70.1.3

Mathematical modelling of induction motors taking into account the design-parameter asymmetry

Petro Kurliak[1],

Valerii Tytiuk[2],

Oleksii Chornyi[3],

Vitaliy Kuznetsov[4],

Artem Artemenko[5],

Olha Chorna[6]

[1] *Department of Electrical Power Engineering, Ivano-Frankivsk National Technical University of Oil and Gas, Ivano-Frankivsk, Ukraine*
Email: petro.kurliak@nung.edu.ua

[2] *Department of Electromechanics, Kryvyi Rih National University, Kryvyj Rih, Ukraine*
Email: tytiuk@knu.edu.ua

[3] *Educational and Research Institute of Electrical Engineering and Information Technologies of Kremenchuk Mykhailo Ostrohradskyi National University, Kremenchuk, Ukraine*
Email: alekseii.chornyi@gmail.com

[4] *Department of Electrical Engineering, Ukrainian State University of Science and Technologies, Dnipro, Ukraine*
Email: v.v.kuznetsov@ust.edu.ua

[5] *Educational and Research Institute of Electrical Engineering and Information Technologies of Kremenchuk, Mykhailo Ostrohradskyi National University, Kremenchuk, Ukraine*
Email: a.m.artemenko@gmail.com

[6] *Educational and Research Institute of Electrical Engineering and Information Technologies, Kremenchuk Mykhailo Ostrohradskyi National University, Kremenchuk, Ukraine*
Email: diolgan@gmail.com

Due to their numerous technical and economic advantages, induction machines (IM) with squirrel-cage rotors are important components of many industrial processes. Their reliability, durability, and ease of operation make them indispensable in various industries, ensuring stable and efficient equipment performance. However, to minimise the risk of costly production failures caused by sudden stoppages, it is important to implement effective diagnostic and monitoring methods. The most common type of fault in squirrel-cage induction motors is the breakage of cage bars and end ring segments, particularly in motors with high inertia loads and frequent stops and starts. Regular maintenance and the implementation of modern control systems in the industry will help ensure the reliable and uninterrupted operation of these machines. In the technical literature, various diagnostic methods have been proposed. Some are based on analysing data collected from the induction motor (IM), detecting characteristic perturbations that indicate faults in the machine. Other methods involve comparing the data obtained from the actual induction motor with its digital model. It is clear that accurate and adequate IM models are necessary for the development and optimisation of fault diagnosis methods. This paper focuses on developing a mathematical model of an induction motor (IM) in a stator-fixed coordinate system, where the squirrel-cage rotor of the IM is represented as a multiphase, symmetrically distributed winding system in space. The adequacy of the obtained model is demonstrated. The developed model allows for the analysis of various types of asymmetries in both stator and rotor of squirrel-cage induction motors

Keywords: induction motor, squirrel-cage, voltage asymmetry, winding asymmetry, broken bar fault

INTRODUCTION

As a rule, the operation of an induction motor (IM) takes place under conditions that are far from ideal, which leads to the necessity of considering various types of asymmetries that adversely affect both operating modes and technical and operational indicators of IM operation.

The most common types of asymmetries that have the most significant effect on IM performance include:

1) asymmetry of supply voltages,
2) parametric asymmetry of stator windings,
3) a break in the rods of the squirrel-cage,
4) local defects of the stator magnetic core.

However, as a rule, the known models of IM do not take possible varieties of the design-parametric asymmetry into account.

The technique of using transformed orthogonal coordinate systems is the most widespread in the practice of mathematical modelling of IM. This approach cannot be used to study IM with the parametric asymmetry of stator or rotor windings, which follows from the applied coordinate transformation technique.

Modelling of IM in the natural system of phase coordinates does not allow for the investigation of operation modes of squirrel-cage induction motors (SCIMs), taking the real design of squirrel-cage rotor into account.

Considering the design-parametric asymmetry, the study of IM operation modes is an important component in the development of IM monitoring and diagnostics systems. Therefore, the task of developing a sufficiently universal model of an induction motor, considering the most important types of the design-parametric asymmetry, is important and urgent.

LITERATURE REVIEW

In [1], the authors propose an algorithm that combines Park's vector approach and its extended variant for detecting and identifying broken rotor bar faults. Detection of this fault is possible using Park's vector approach by observing the thickness and orientation of Park's vector pattern.

In [2], an approach is proposed where faults in the bearing of a three-phase IM are detected by selecting frequencies in the stator current spectrum.

In [3], a method is proposed for detecting broken bar faults and assessing their severity during start-up conditions. The approach involves using successive variable mode decomposition along with quadratic regression of the squared instantaneous frequency to analyse the stator starting current and extract the fault components.

A method of using deep neural networks for monitoring stator and rotor damage is dealt with in [4], while [5] explores the application of information entropy analysis to the electrical current supplied to an IM during both start-up and steady-state conditions.

In [6], the potential of using Least Squares Support Vector Machines (LS-SVM) for detecting partial ruptures in rotor bars of squirrel-cage induction machines is explored. The study employs spectral analysis of the stator current using the Fast Fourier Transform (FFT) method to identify fault frequencies associated with these partial ruptures in the rotor bars of squirrel-cage IMs.

A method for detecting broken rotor bars in a three-phase squirrel-cage induction motor using vibration signals combined with Higher-Order Statistics and machine learning methods is proposed in [7], and [8] suggests using cascaded neural structures for detecting electrical circuit damage in an induction motor with a frequency converter. The diagnosis of induction machines using artificial neural networks based on the analysis of stator current as input features is addressed in [9]. The paper provides a comparison of the effectiveness of different types of artificial neural network (ANN) classifiers in detecting faults in asynchronous machines (rotor and bearing faults).

Application of the discrete wavelet transform (DWT) method with the analysis of stator current in SCIM for detecting broken rotor bars is discussed in [10].

The focus in [11] is on the problem of detecting rotor asymmetry faults using modified motor current signature analysis, which is based on advanced time-frequency transforms such as the continuous wavelet transform.

A new method for analytical modelling of induction motors with asymmetrical cage windings using a tensor-based approach is

proposed in [12]. It greatly simplifies the process by applying standard tensor algebra.

The issues of mathematical modelling of induction motors in the phase coordinate system, allowing for the consideration of various types of stator winding asymmetry, are investigated in [13]. However, the proposed model does not allow for examining the actual design of a short-circuited rotor in the form of a closed multi-bar squirrel-cage.

A computer-integrated system designed for automatic control in centrifuges with variable imbalance is introduced in [14]. The system utilises a computer-oriented Bond Graph model of an induction motor with a squirrel-cage rotor.

[15] is the first to thoroughly investigate the paths of voltage sag propagation, covering all four types of short-circuits and their connections with other grid events (interruptions, transients, imbalances).

Finally, [16] proposes using mathematical models to forecast the values of key indicators of energy efficiency and operational reliability of electrical systems and motors, as well as their energy parameters, in order to select the optimal operating mode. For this purpose, the spectra of current and asymmetry are measured at the terminals of the motors.

MATERIALS OF THE STUDY

The issue of accounting for the complex design of a short-circuited rotor in the form of a closed multi-rod squirrel-cage is relatively little investigated. Figure 1 displays the diagram of a healthy squirrel-cage induction motor. In it, vertical lines represent the rotor bars and horizontal lines depict the end rings. Two rotor bars and their connections are shown as a single circuit, with independent currents flowing through each loop, and all loops being equal. The rotor current loop is denoted as i_{rk}, which varies across different bars. The i_{rk} is the current in the rotor circuit.

To investigate the influence of breakage of the rotor squirrel-cage rods on IM operation, we used the representation of the IM rotor as a system of multiphase windings, in which each rotor rod was considered as a separate winding.

To derive the equations of the theoretical mathematical model of an IM with a multiphase rotor, we applied the theory of the generalised electromechanical converter.

In deriving the equations, we used the commonly accepted assumptions associated with the concept of an idealised engine:

- unsaturated engine steel,
- the stator phase windings are uniformly distributed in space,
- rods of the squirrel-cage of the rotor are uniformly distributed in space,
- distributed windings in reality are replaced with concentrated windings, and the magneto-motive force (MMF) is assumed to match the MMF of the actual winding,
- the winding and magnetic fields propagate sinusoidally along the circumference of the air gap.

Let us represent the IM as a system of magnetically coupled windings. For the sake of generality, we will assume that the stator winding is a multiphase winding. On the stator, there are M-windings connected to the M-phase power supply. On the rotor, there are N short-circuited windings, where N equals to the number of squirrel-cage rods (Fig. 2).

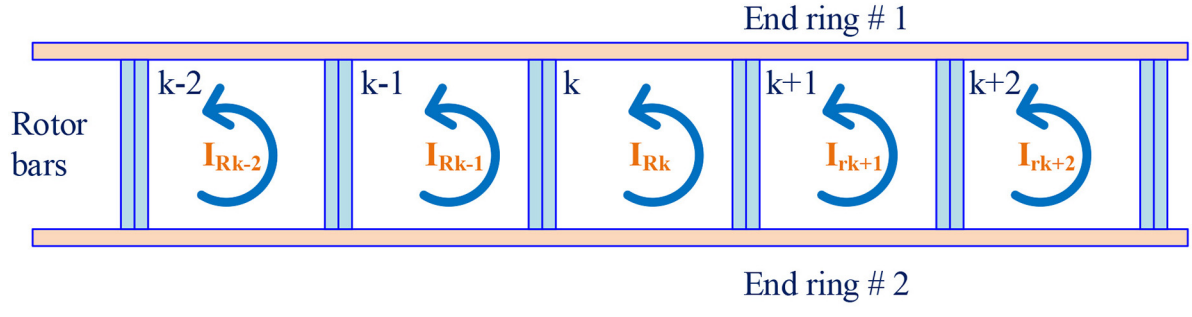

Fig. 1. Modelling of a healthy squirrel-cage induction motor

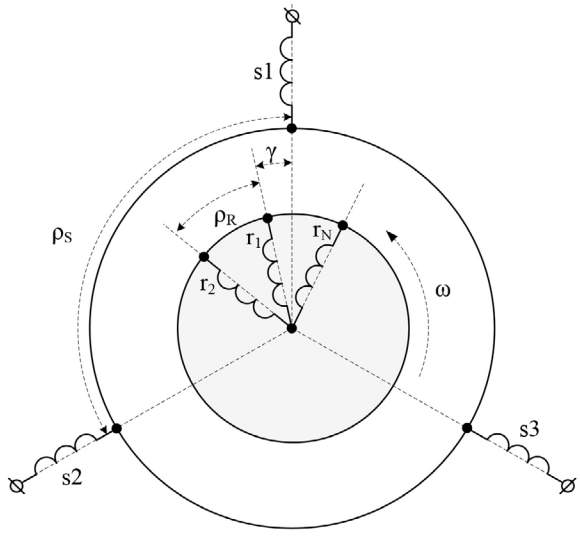

Fig. 2. Scheme of mutual arrangement of stator and rotor windings of a multiphase IM for the case of the number of stator phases $M = 3$

The system of equations of electrical equilibrium of a motor with a multiphase rotor in matrix form will have a known form:

$$[\mathrm{U}] = [\mathbf{R}] \cdot [\mathbf{I}(t)] + \frac{d}{dt}\{\boldsymbol{\psi}(t)\} \quad (1)$$

The following notations are adopted in this equation:

The vector-column of stator supply voltages has dimension M:

$$[\mathbf{U}_S] = [U_1\ U_2 \ldots U_M]^T. \quad (2)$$

Let us introduce additional notations:

$$\rho_S = 2\pi/M;\ \rho_R = 2\pi/N. \quad (3)$$

Then, the stator supply voltage in a general form can be written as follows:

$$U_k = \sqrt{2} \cdot U_f \cdot sin\left(\omega_C \cdot t - \rho_S \cdot (k-1)\right), \quad (4)$$

where $\omega_C = 2\pi \cdot f \cdot p$ is the angular speed of rotation of the stator field with the frequency of the supply network f at the number of pole pairs p.

The supply voltage column vector for a squirrel-cage rotor is a zero vector of dimension N.

$$[\mathbf{U}_R] = [0\ 0 \ldots 0]^T. \quad (5)$$

Then the vector-column of supply voltages in cell-matrix form is

$$\mathbf{U} = \begin{bmatrix} \mathbf{U}_S \\ \hline \mathbf{U}_R \end{bmatrix}, \quad (6)$$

and has dimension $M+N$.

Similarly, the vector-column of stator winding currents has dimension M:

$$[\mathbf{I}_S] = [I_1\ I_2 \ldots I_M]^T. \quad (7)$$

Vector-column of rotor winding currents of dimension N:

$$[\mathbf{I}_R] = [I_{R1}\ I_{R1} \ldots I_{RN}]^T. \quad (8)$$

Vector-column of currents in cell-matrix form is equal to

$$\mathbf{I} = \begin{bmatrix} \mathbf{I}_S \\ \hline \mathbf{I}_R \end{bmatrix}. \quad (9)$$

The square diagonal matrix of active resistances [**R**] has dimension $(M+N) \times (M+N)$. The elements of the main diagonal of this matrix are equal to the active resistances of the corresponding windings, which allows the modelling of the operation modes of IMs with asymmetrical active resistances.

Similarly to the currents, the column vector of stator winding fluxes has dimension M:

$$[\boldsymbol{\Psi}_S] = [\Psi_1\ \Psi_2 \ldots \Psi_M]^T. \quad (10)$$

Vector-column of the rotor winding fluxes of dimension N:

$$[\boldsymbol{\Psi}_R] = [\Psi_{R1} \Psi_{R2} \ldots \Psi_{RN}]^T. \quad (11)$$

The vector-column of fluxes in the cell-matrix form is equal to

$$\boldsymbol{\Psi} = \begin{bmatrix} \boldsymbol{\Psi}_S \\ \hline \boldsymbol{\Psi}_R \end{bmatrix}. \quad (12)$$

The flux equation for each winding can be written in the form:

$$\Psi_k = I_k \cdot L_k + \sum\nolimits_{j=1}^{j=N, j\neq k} I_j \cdot M_{kj}, \quad (13)$$

where ψ_k, I_k, L_k are the flux-coupling, current and inductance of the winding with index k; I_j, M_{kj}

current of the j-th circuit and mutual inductance of windings with indices *k* and *j*.

The currents of each winding can be divided into two components: those formed by the currents of windings that are stationary, relative to each other, and those of windings that rotate relative to each other at rotor speed.

The stator winding eigeninductance matrix can be written in the following form:

$$[\mathbf{L}_{SS}] = [\mathbf{L}_{\delta S}] + [\mathbf{M}_{SS}], \quad (14)$$

where $\mathbf{L}_{\delta S}$ is a square diagonal matrix of intrinsic dissipation inductances of dimension $M \times M$; the elements of the main diagonal of this matrix are equal to the dissipation inductances of the stator windings; $\mathbf{M}_{SS}$ is a square matrix of mutual inductances between the stator windings of dimension $M \times M$; the elements of this matrix are equal to the mutual inductances between the corresponding stator windings. Since the stator windings are shifted in space relative to each other by the value ρ_S, the expression of the mutual inductance between the stator windings with indices *j* and *k* can be written as follows:

$$\mathbf{M}_{SS}[j, k] = m_1 \cdot \cos(\rho_S \cdot (k - j)); \quad j = 1 \ldots M; k = 1 \ldots M. \quad (15)$$

The individual terms of (14) in the expanded form are as follows

where $l_{1\delta}$ – dissipation inductance of stator phase of IM stator; m_1 – maximum value of mutual inductance between stator phases.

$$\mathbf{L}_{\delta S} = \begin{bmatrix} l_{1\delta} & 0 & \cdots & 0 & 0 \\ 0 & l_{1\delta} & \cdots & 0 & 0 \\ \cdots & \cdots & \cdots & \cdots & \cdots \\ 0 & 0 & \cdots & l_{1\delta} & 0 \\ 0 & 0 & \cdots & 0 & l_{1\delta} \end{bmatrix}; \quad (16)$$

$$\mathbf{M}_{\delta SS} = \begin{bmatrix} m_1 \cdot cos(\rho_S \cdot (1-1)) & m_1 \cdot cos(\rho_S \cdot (2-1)) & \cdots & m_1 \cdot cos(\rho_S \cdot (M-1-1)) & m_1 \cdot cos(\rho_S \cdot (M-1)) \\ m_1 \cdot cos(\rho_S \cdot (1-2)) & m_1 \cdot cos(\rho_S \cdot (2-2)) & \cdots & m_1 \cdot cos(\rho_S \cdot (M-1-2)) & m_1 \cdot cos(\rho_S \cdot (M-2)) \\ \cdots & \cdots & \cdots & \cdots & \cdots \\ m_1 \cdot cos(\rho_S \cdot (1-(M-1))) & m_1 \cdot cos(\rho_S \cdot (2-(M-1))) & \cdots & m_1 \cdot cos(\rho_S \cdot (M-1-(M-1))) & m_1 \cdot cos(\rho_S \cdot (M-(M-1))) \\ m_1 \cdot cos(\rho_S \cdot (1-M)) & m_1 \cdot cos(\rho_S \cdot (2-M)) & \cdots & m_1 \cdot cos(\rho_S \cdot (M-1-M)) & m_1 \cdot cos(\rho_S \cdot (M-M)) \end{bmatrix}.$$

Similarly, taking into account the number of rotor phases, the own inductance matrices of the rotor windings can also be represented thus:

$$[\mathbf{L}_{RR}] = [\mathbf{L}_{\delta R}] + [\mathbf{M}_{RR}], \quad (17)$$

where $\mathbf{L}_{\delta R}$ is a square diagonal matrix of intrinsic dissipation inductances of dimension $N \times N$; elements of the main diagonal of this matrix are equal to dissipation inductances of rotor windings; $\mathbf{M}_{RR}$ is a square matrix of mutual inductances between rotor windings of dimension $N \times N$; elements of this matrix are equal to mutual inductances between corresponding rotor windings. Since the rotor windings are shifted in space relative to each other by the value ρ_R, the expression of the mutual inductance between the rotor windings with indices *j* and *k* can be written as follows:

$$\mathbf{M}_{RR}[j,k] = m_2 \cdot \cos(\rho_R \cdot (k-j)); j = 1 \ldots N; k = 1 \ldots N. \quad (18)$$

Next, a matrix of mutual inductances between the stator windings and the rotating rotor windings must be compiled.

Based on geometrical considerations, in Fig. 1, the formula for the mutual inductance between the rotor winding with number n and the stator winding with number m can be written as follows:

$$\mathbf{M}_{SmRn} = m_0 \cdot \cos(\gamma(t)) - \rho_S(m-1) + \rho_R(n-1)), \quad (19)$$

where m_0 is the maximum value of mutual inductance between stator and rotor windings at the coincidence of their axes; $\gamma(t)$ is the instantaneous value of rotor rotation angle.

The matrix of mutual inductances between the stator and rotor windings will generally be a rectangular matrix of dimension $M \times N$.

Then the full matrix of mutual inductances of a multiphase IM can be represented in the following cell-matrix form:

$$\mathbf{M} = \left[\begin{array}{c|c} \mathbf{L}_{SS} & \mathbf{M}_{SR} \\ \hline \mathbf{M}_{SR}^{T} & \mathbf{L}_{RR} \end{array}\right]. \tag{20}$$

This matrix is square and has dimension $(M+N) \times (M+N)$.

The torque of an induction motor can be calculated as follows [14]:

$$\begin{aligned} T_E = \frac{Z_p}{\sqrt{3}}\big[\Psi_A\left(I_B - I_C\right) + \\ + \Psi_B\left(I_C - I_A\right) + \Psi_C\left(I_A - I_B\right)\big], \end{aligned} \tag{21}$$

or by a more general expression

$$\begin{aligned} T_E = -\frac{3}{2} Z_p \cdot \left(\vec{\Psi}_1 \times \vec{\mathbf{I}}_1\right) = \\ = -\frac{3}{2} Z_p \cdot \left(\left|\vec{\Psi}_1\right| \cdot \left|\vec{\mathbf{I}}_1\right| \cdot sin\left(\alpha_\Psi - \alpha_\mathbf{I}\right)\right). \end{aligned} \tag{22}$$

The space vectors of stator flux-current and current can be determined from their instantaneous values, taking into account the phase shift of flux-current and current values of individual phases of the induction motor:

$$\vec{\mathbf{I}}_1 = \sum_{k=1}^{N} I_k \cdot e^{i(k-1)}. \tag{23}$$

The equation for describing the motion of the rotating parts of an induction motor is derived from the principle of conservation of momentum. When the moment of inertia remains constant, this equation is analogous to Newton's second law for rotational motion:

$$T_E - T_L = J \frac{d\omega_r}{dt}, \tag{24}$$

where T_E – electromagnetic torque of electric motor, Nm; T_L – load torque, Nm; J – moment of inertia, Nm; ω_r – angular speed of the engine rotor, s^{-1}; t – time, s.

REALISATION OF THE MATHEMATICAL MODEL OF IM IN MATLAB

For mathematical modelling of asymmetrical modes of IM, the induction motor type 4A90 L2 (Ukraine) with the following technical characteristics was used:

Table 1. **Parameters of the induction motor type 4A90 L2**

Rated power, kW	3.0
Rated voltage, V	380
Rated stator current, A	6.4
Rated speed, rpm	2860
Nominal efficiency factor	0.845
Rated power factor	0.88
Efficiency factor at 75% utilisation	0.855
Power factor at 75% load IM	0.85
Inrush current multiplicity	6.0
Overload capability	2.5
Moment of inertia, kGm^2	0.0049
Number of rotor bars	20

Table 2. **Parameters of the T-substitution diagram**

4A90 L2	R_1	R_2	X_1	X_2	X_M
Catalogue, ohm	2.4943	1.6282	1.9747	3.464	117.7871
Calculation, ohm	2.3576	1.7783	2.9516	3.9878	104.405

The solution of the proposed equations was implemented using LiveScript technology in MATLAB. The ODE45 solver with relative tolerance 1e-6 and maximal integration step 0.0005 was used for the numerical solution of the proposed equations of SCIM.

To check the adequacy of the developed mathematical model using MATLAB, the solutions for the standard configuration of SCIM with three-phase symmetrical windings on the stator and rotor were obtained. The obtained solutions are presented in Fig. 3.

The obtained diagrams show that the stator inrush current, the magnetising current, and the rated current coincide with the nameplate values, which makes us optimistic about the adequacy of the model.

Figure 4 shows similar diagrams for SCIM with the multiphase rotor, $N = 20$.

As follows from the given graphs, the values of stator currents, performance indicators of the

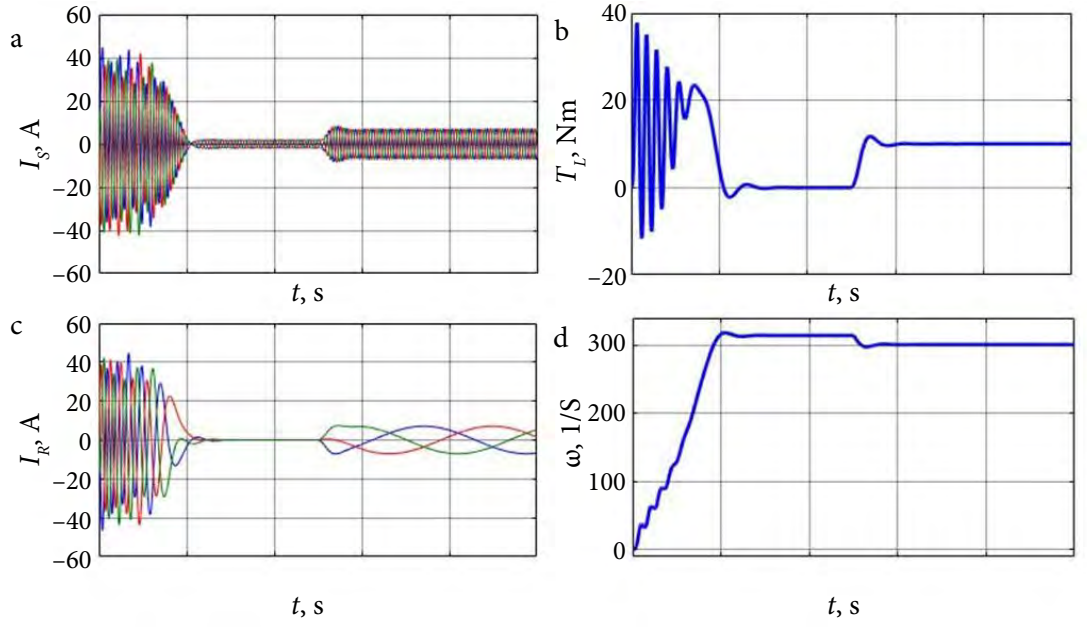

Fig. 3. Diagrams of starting and charging of nominal load ($t = 0.5$ c), obtained for SCIM with the number of rotor phases $N = 3$: a – stator currents; b – rotor currents; c – electromagnetic torque; d – angular velocity

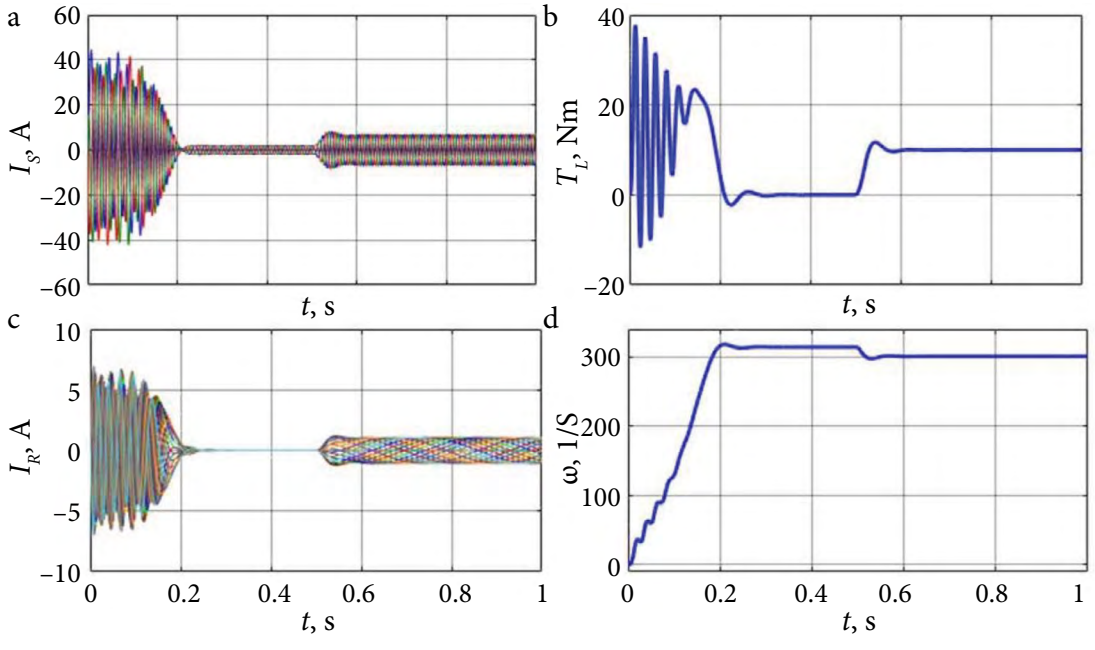

Fig. 4. Diagrams of starting and charging of nominal load ($t = 0.5$ c), obtained for SCIM with the number of rotor phases $N = 20$: a – stator currents; b – rotor currents; c – electromagnetic torque; d – angular velocity

mechanical part of the SCIM do not change, which is an indirect confirmation of the correctness of the developed model.

For convenience of visualisation of the currents shape, the hodographs of space vectors for the stator and rotor currents were constructed. As it could be expected, in the symmetric mode of operation, the hodographs of space vectors for the stator and rotor currents were circles with the centre at the origin, Fig. 5.

Figure 6 shows diagrams of stator phase currents in quasi-steady operation mode with un-

Godograph of starter current

of rotor current

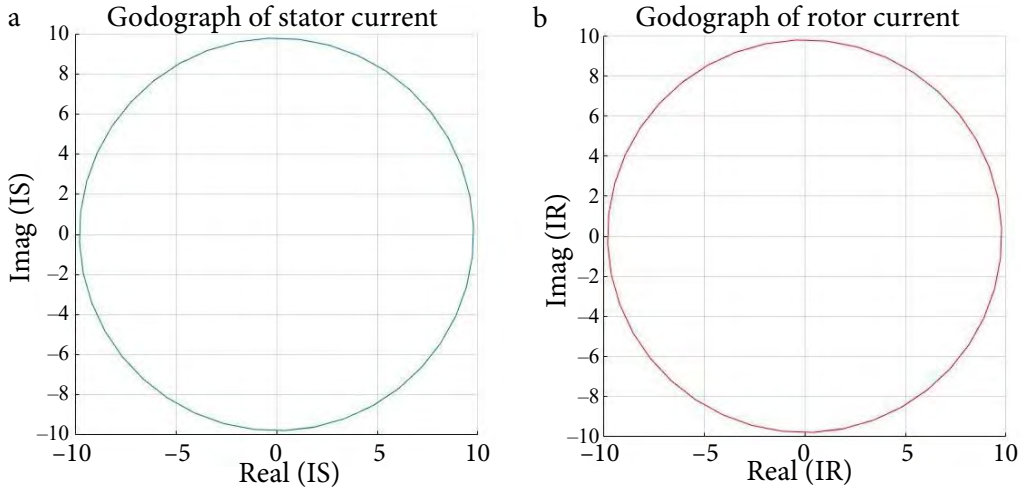

Fig. 5. Hodographs of space vectors for stator and rotor currents: a – the hodograph of the stator current vector; b – the hodograph of the rotor current vector

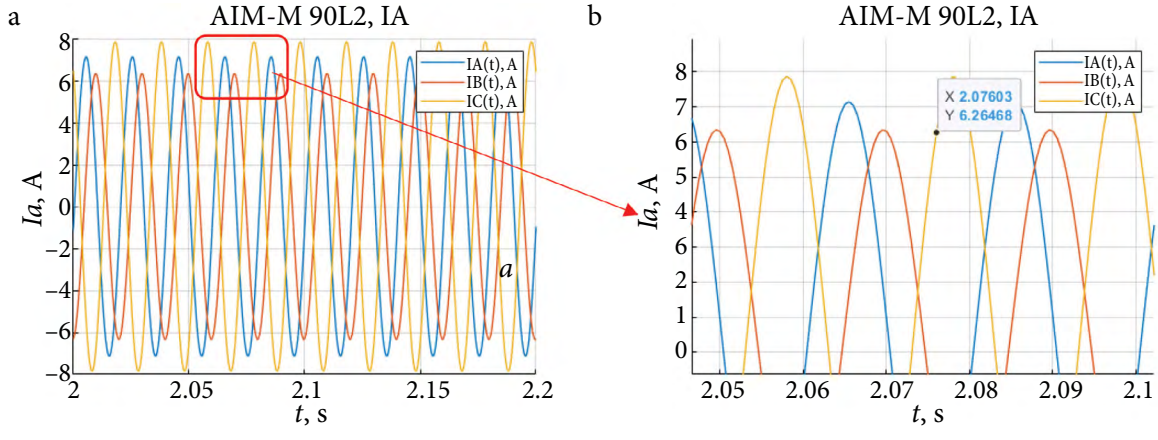

Fig. 6. SCIM stator currents under stator supply voltage asymmetry: a – stator currents at unbalanced supply voltage in phase B; b – stator currents at unbalanced supply voltage in phase B, enlarged

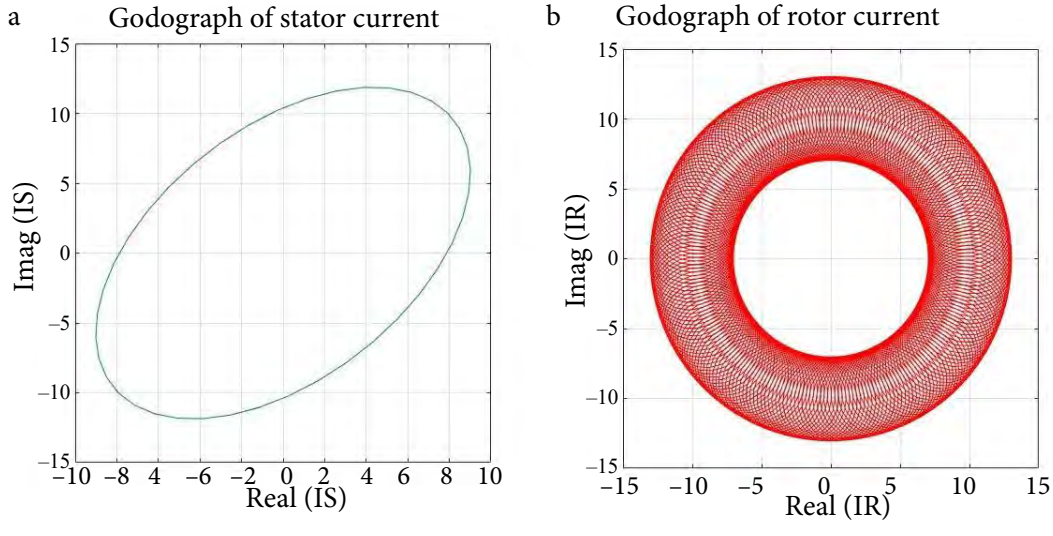

Fig. 7. Hodographs of space vectors for stator and rotor currents at unbalanced supply voltage: a – the hodograph of the stator current vector; b – the hodograph of the rotor current vector

balanced stator voltage. In the computational experiment, it was assumed that the stator phase B voltage is 90% of the nominal voltage. Graphs Fig. 6a, 6b clearly show the differences in phase currents caused by this type of asymmetry.

Also, there are pulsations of the electromagnetic torque of IM and asymmetrical distribution of currents in rotor bars.

Figure 7 shows the hodographs of space vectors for stator and rotor currents at unbalanced supply voltages.

Figure 8 shows the diagrams of stator phase currents in quasi-steady operation mode with a winding fault in one of the stator phases. In the computational experiment, 30% of turns in the stator phase B were assumed to be damaged. Graphs a and b in Fig. 8 show the differences in phase currents caused by this type of asymmetry.

Figure 9 shows the hodographs of the space vectors for the stator and rotor currents at the winding in phase B of the stator.

Let us investigate the operation of SCIM at rotor rod breakage. The operation of SCIM starts from a fully symmetrical, serviceable state. After starting at idle, load build-up occurs at the moment of time t = 1s. After the onset of a steady state operation with nominal load at t = 2s, the rotor rod break occurs, and the motor enters

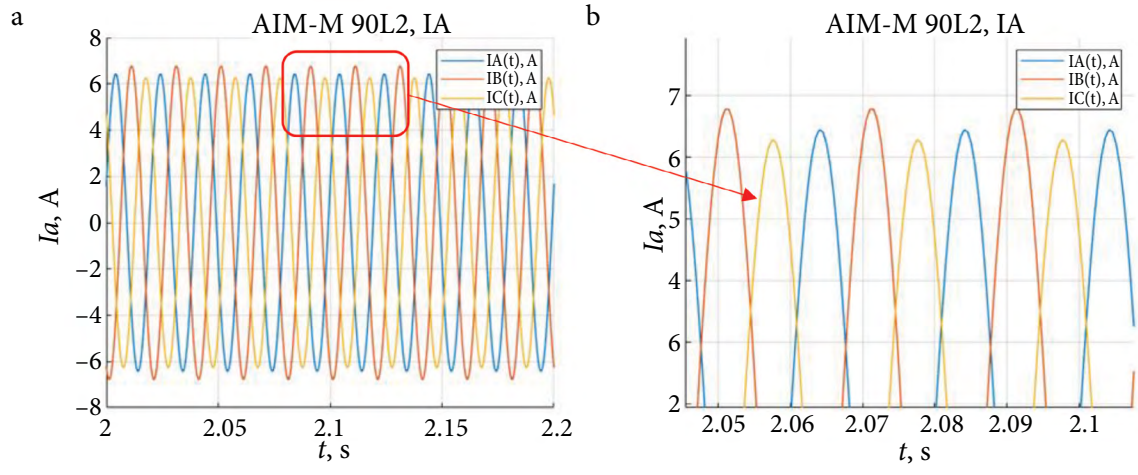

Fig. 8. SCIM stator currents under turn-to-turn short circuit of the stator winding: a – stator currents, short circuit in phase B; b – stator currents, short circuit in phase B, enlarged

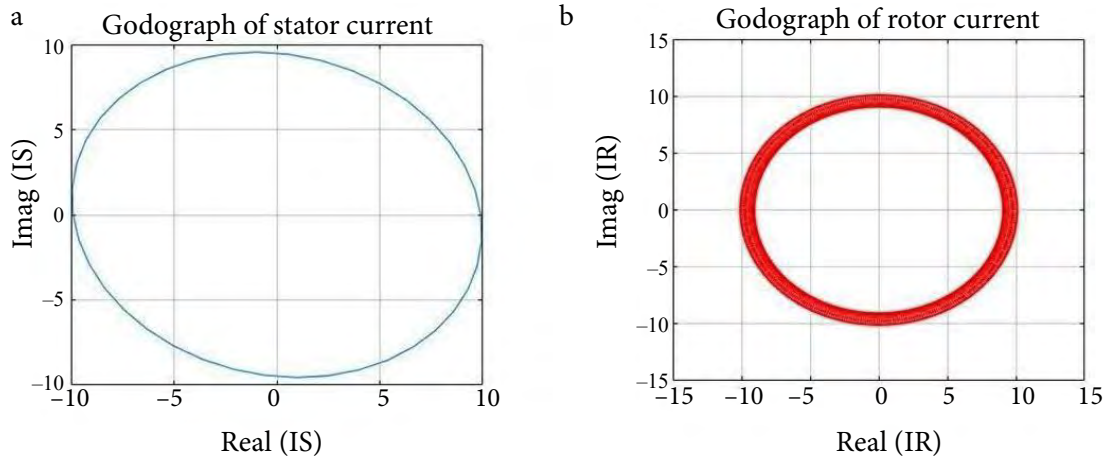

Fig. 9. Hodographs of space vectors for stator and rotor currents at winding fault in phase B of the stator: a – the hodograph of the stator current vector; b – the hodograph of the rotor current vector

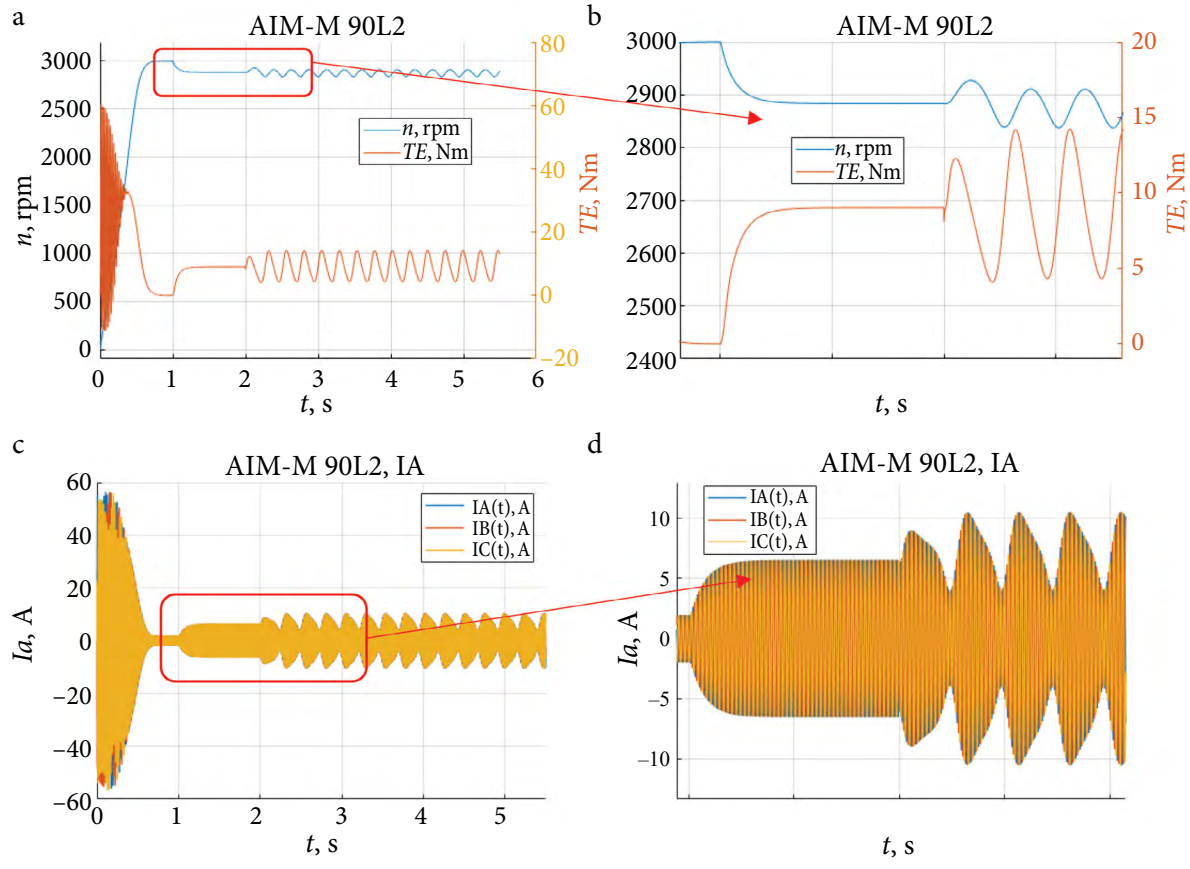

Fig. 10. Study of SCIM operation at rod breakage in the rotor: a – electromagnetic torque and speed of the motor drive; b – electromagnetic torque and rotation speed of the SCIM motor, enlarged; c – SCIM stator currents; d – SCIM stator currents, enlarged

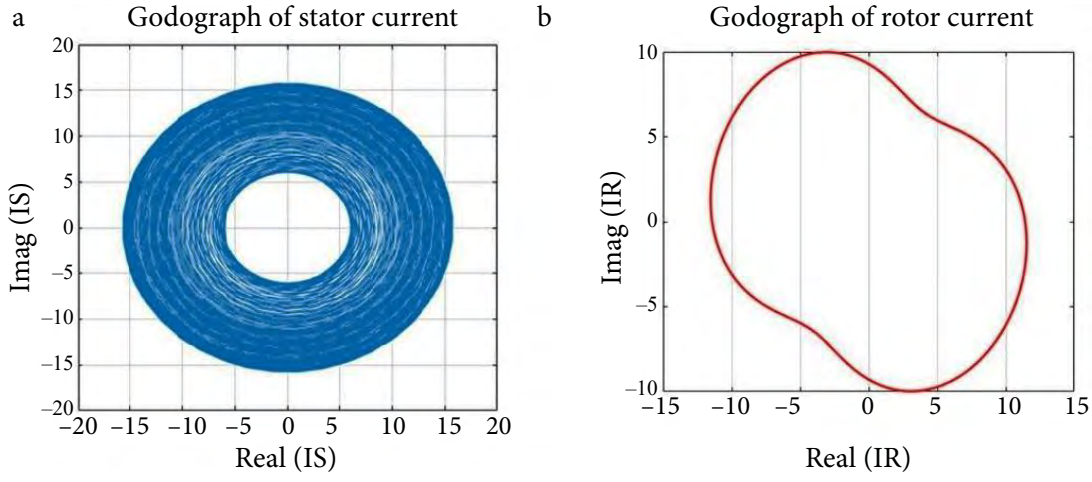

Fig. 11. Hodographs of space vectors for stator and rotor currents at rod break in the rotor: a – the hodograph of the stator current vector; b – the hodograph of the rotor current vector

the auto-oscillating mode. The described results are presented in Figs 10 and 11.

Figure 11 shows the hodographs of the space vectors for the stator and rotor currents at the rod break in the rotor.

It draws attention to the fact that the appearance of the stator current hodograph available for measurements has a rather different appearance for different asymmetrical modes, which can be used in the further development

of methods for identification of different IMs faults.

CONCLUSIONS

A theoretical mathematical model of induction motor with multiphase stator winding and squirrel-cage rotor in a coordinate system fixed relative to the stator is developed. The proposed model differs from the known ones in that the squirrel-cage of the IM rotor is represented by a multiphase winding system symmetrically distributed in space. It allows using the developed model for analysis of asymmetrical modes of SCIM at various types of stator and rotor asymmetry and their combinations. The adequacy of the proposed mathematical model is substantiated. Calculations of steady-state modes of SCIM operation in asymmetrical modes of various types of operation, including rotor bar breakage, are given. The possibility of using the geometrical properties of the stator current hodograph for identification of the type of IMs fault is shown.

Received 19 March 2024
Accepted 8 August 2024

References

1. Messaoudi M., Flah A., Alotaibi A. A., Althobaiti A., Sbita L., Ziad El-Bayeh C. Diagnosis and fault detection of rotor bars in squirrel-cage induction motors using combined Park's vector and extended Park's vector approaches. *Electronics*. 2022. Vol. 11. No. 3. ID 380. https://doi.org/10.3390/electronics11030380
2. Pandarakone S. E., Mizuno Y., Nakamura H. Distinct Fault analysis of induction motor bearing using frequency spectrum determination and support vector machine. *IEEE Trans. Industry Applications* Vol. 11. No. 3, May–June 2017. P. 3049–3056. https://doi.org/10.1109/TIA.2016.2639453
3. Liu X., Yan Y., Hu K., Zhang S., Li H., Zhang Z., Shi T. Fault diagnosis of rotor broken bar in induction motor based on successive variational mode decomposition. *Energies*. 2022. Vol. 15. No. 3. ID 1196. https://doi.org/10.3390/en15031196
4. Skowron M. Application of deep learning neural networks for the diagnosis of electrical damage to the induction motor using the axial flux. Bulletin of the Polish Academy of Sciences. *Technical Sciences*. 2020. Vol. 68. No. 5. P. 1031–1038. https://doi.org/10.24425/bpasts.2020.134664
5. S. Tierrafria-Baez P. M., Calderon-Lopez V., Cano-Valdez B. K., Aviles-Diaz C., Rodriguez-Donate E. Cabal-Yepez, Broken rotor bar detection in induction motors through information entropy analysis on the start-up transient and steady-state current signals. *IECON 2021 – 47th Annual Conference of the IEEE Industrial Electronics Society*, 2021. P. 1–6, https://doi.org/10.1109/IECON48115.2021.9589669
6. Birame M'hamed, Bessedik Sid Ahmed, Benkhoris Mohamed Fouad. Detection of partial rotor bar rupture of a cage induction motor using least square support vector machine approach. *Diagnostyka*. 2021. Vol. 22. No. 1. P. 57–63. https://doi.org/10.29354/diag/133039
7. Medeiros M., Nascimento N., Silva S. P. P., Reboucas Filho P. P., Marques Sa Medeiros C. Higher-Order Statistics applied to machine learning as an approach to identify broken rotor bars in induction motors. *IEEE Latin America Transactions*. Vol. 16. No. 8, August 2018. P. 2267–2274. https://doi.org/10.1109/TLA.2018.8528245
8. Skowron M., Orłowska-Kowalska T. Efficiency of cascaded neural networks in detecting initial damage to induction motor electric windings. *Electronics*. 2020. Vol. 9. ID 1314. https://doi.org/10.3390/electronics9081314
9. Sameh M., Tarek A., Yassine K. Bearing and rotor faults detection and diagnosis of induction motors using statistical neural networks. *20th International Conference on Sciences and Techniques of Automatic Control and Computer Engineering (STA)*, December 20–22. 2020. P. 77–81. https://doi.org/10.1109/STA50679.2020.9329334
10. Sinha A. K., Hati A. S., Benbouzid M., Chakrabarti P. ANN-based pattern recognition for induction motor broken rotor bar monitoring under supply frequency regulation. *Machines*. 2021. Vol. 9. No. 5. ID 87. https://doi.org/10.3390/machines9050087
11. Puche-Panadero R., Martinez-Roman J., Sapena-Bano A., Burriel-Valencia J., Riera-Guasp M. Fault Diagnosis in the slip-frequency plane of induction machines working in time-varying con-

ditions. *Sensors.* 2020. Vol. 20. No. 12. ID 3398. https://doi.org/10.3390/s20123398

12. Martinez-Roman J., Puche-Panadero R., Sapena-Bano A., Terron-Santiago C., Burriel-Valencia J., Pineda-Sanchez M. Analytical model of induction machines with multiple cage faults using the winding tensor approach. *Sensors*. 2021. Vol. 21. No. 15. ID 5076. https://doi.org/10.3390/s21155076
13. Tytiuk V., Pozigun O., Chornyi O., Berdai A. Identification of the active resistances of the stator of an induction motor with stator windings dissymmetry. *Proceedings of the International Conference on Modern Electrical and Energy Systems* (*MEES) 2017*. P. 48–51. https://doi.org/10.1109/MEES.2017.8248949
14. Pavlenko V., Kurliak P., Batsala Y., Dromenko V., Volianyk O., Horiashchenko S. Computer-integrated drive control in systems with variable imbalance. *2023 IEEE 4th KhPI Week on Advanced Technology (KhPIWeek), October 02–06, 2023*, *Kharkiv, Ukraine.* P. 1–5. https://doi.org/10.1109/KhPIWeek61412.2023.10312999
15. Liubčuk V., Radziukynas V., Kairaitis G., Naujokaitis D. Power quality monitors displacement based on voltage sags propagation mechanism and grid reliability indexes. *Applied Sciences*. 2023. Vol. 13. No. 21. id 11778. https://doi.org/10.3390/app132111778
16. Fedoriv M. Y., Gladj I. V., Galushchak I. D., Batsala Y. V. Increasing reliability and energy efficiency of electrically driven drilling units. *Naukovyi visnyk NGU*. 2017. Vol. 2. P. 93–98. http://nbuv.gov.ua/UJRN/Nvngu_2017_2_16

Petro Kurliak, Valerii Tytiuk, Oleksii Chornyi, Vitaliy Kuznetsov, Artem Artemenko, Olha Chorna

INDUKCINIŲ MOTORŲ MATEMATINIS MODELIAVIMAS ATSIŽVELGIANT Į KONSTRUKCINIŲ PARAMETRŲ ASIMETRIJĄ

Santrauka

Indukciniai motorai (IM) su narveliniais rotoriais yra svarbūs komponentai daugelyje pramonės procesų dėl įvairių techninių ir ekonominių pranašumų. Jie yra patikimi, ilgaamžiai ir patogūs, todėl juos galima naudoti įvairiose pramonės šakose, užtikrinant stabilų ir efektyvų įrangos veikimą. Tačiau, norint sumažinti brangiai kainuojančių gamybos sutrikimų dėl staigių sustojimų riziką, svarbu taikyti veiksmingus diagnostikos ir stebėsenos metodus. Dažniausiai pasitaikantis asinchroninių variklių su narveliniu rotoriumi gedimo tipas yra narvelinių strypų ir galinių žiedų segmentų lūžimas, ypač varikliuose, kurių inercijos apkrova didelė ir kurie dažnai stabdomi ir paleidžiami. Nuolatinė techninė priežiūra ir modernių valdymo sistemų diegimas pramonėje padės užtikrinti patikimą ir nepertraukiamą šių mašinų veikimą. Techninėje literatūroje siūlomi įvairūs diagnostikos metodai. Kai kurie iš jų grindžiami IM surinktų duomenų analize, aptinkant būdingus trikdžius, rodančius mašinos gedimus. Taikant kitus metodus duomenys, gauti iš realaus indukcinio variklio, lyginami su jo skaitmeniniu modeliu. Akivaizdu, kad tikslūs ir tinkami IM modeliai yra būtini gedimų diagnostikos metodams kurti ir optimizuoti. Šiame straipsnyje daugiausia dėmesio skiriama indukcinio motoro matematinio modelio sukūrimui statoriaus fiksuotoje koordinačių sistemoje, kur IM narvelinis rotorius vaizduojamas kaip daugiafazė simetriškai erdvėje paskirstyta apvijų sistema. Įrodytas gauto modelio tinkamumas. Sukurtas modelis leidžia analizuoti įvairių tipų asimetriją tiek narvelinio rotoriaus indukcinių variklių statoriuje, tiek rotoriuje.

Raktažodžiai: indukcinis motoras, narvelinis rotorius, įtampos asimetrija, apvijos asimetrija, lūžtančio strypo gedimas